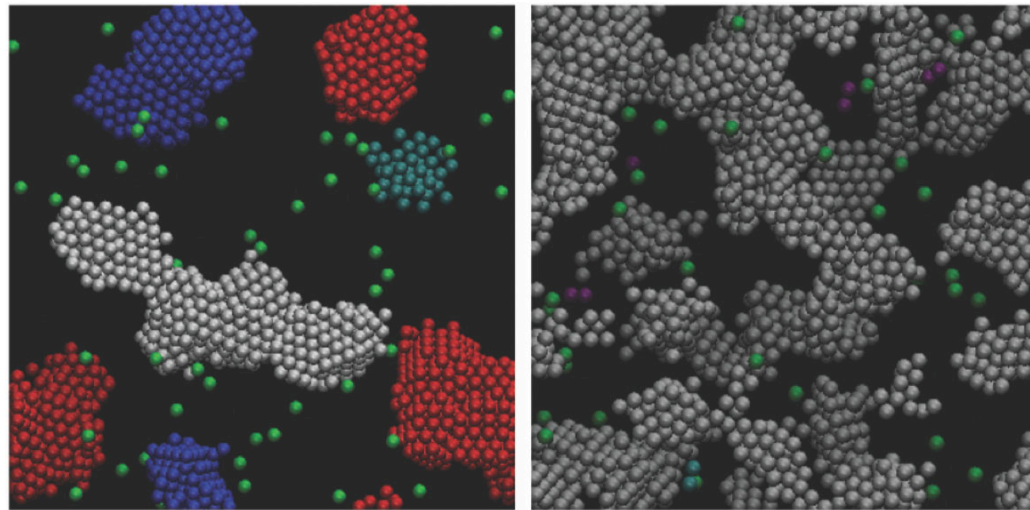
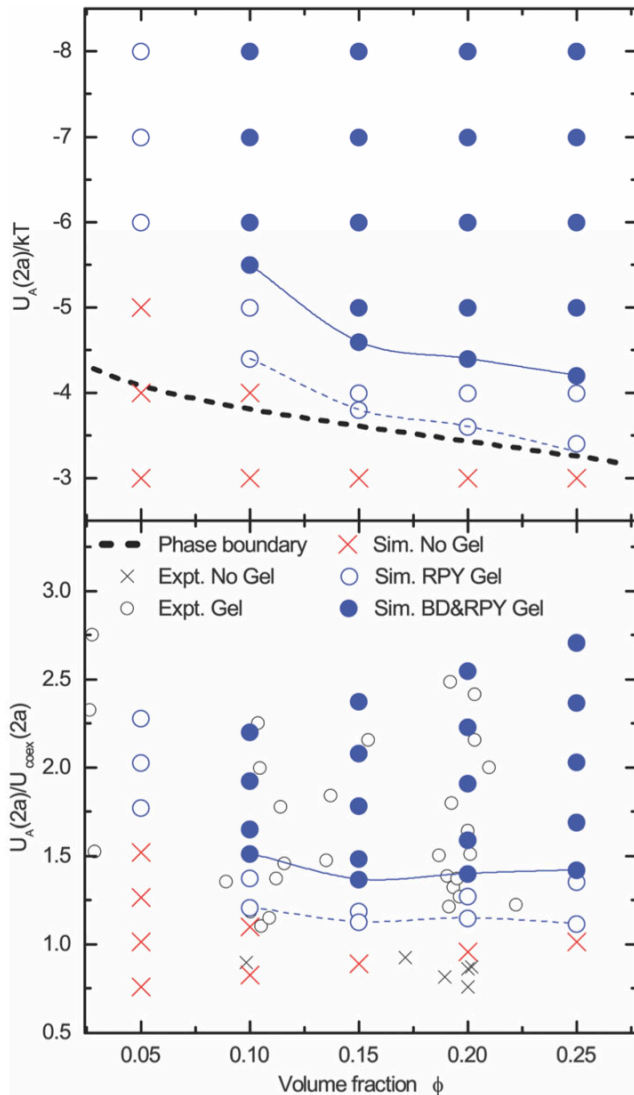


Structure in flows

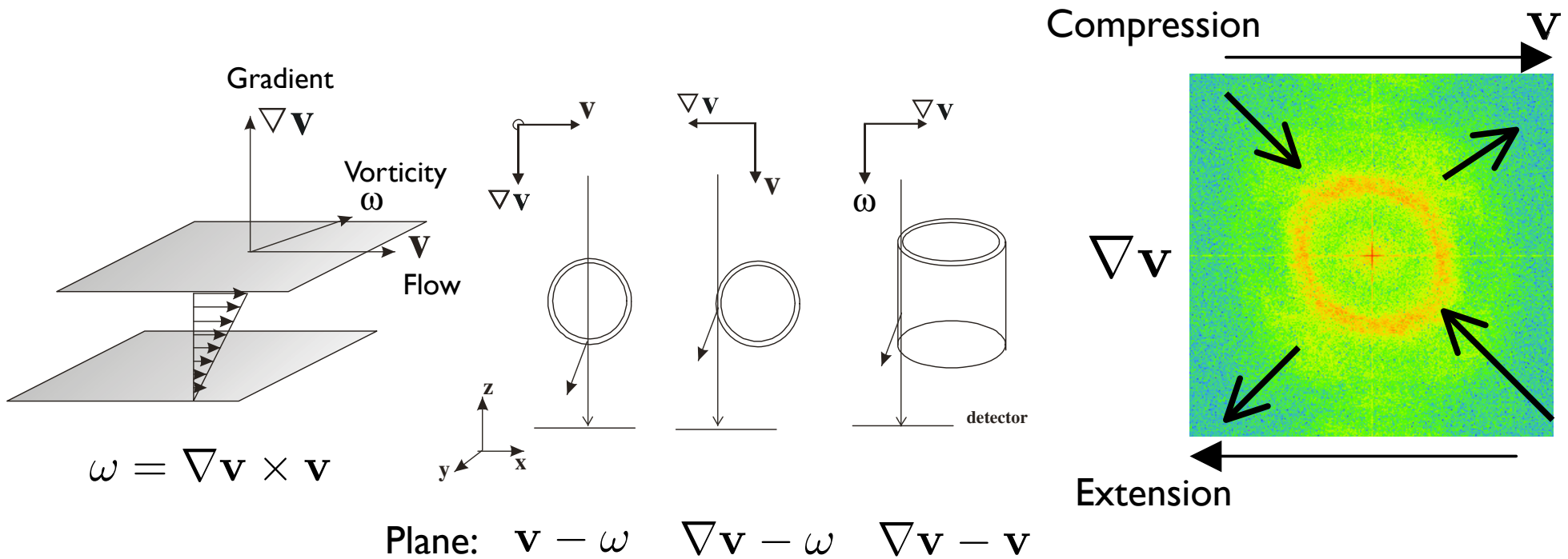
Hydrodynamic interactions

Varga, Z., Wang, G. & Swan, J. The hydrodynamics of colloidal gelation. *Soft Matter* 11, 9009–9019 (2015).



Structure in flow

J. Vermant and M. J. Solomon, J. Phys.: Condens. Matter 17, R187 (2005).

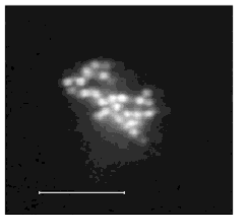
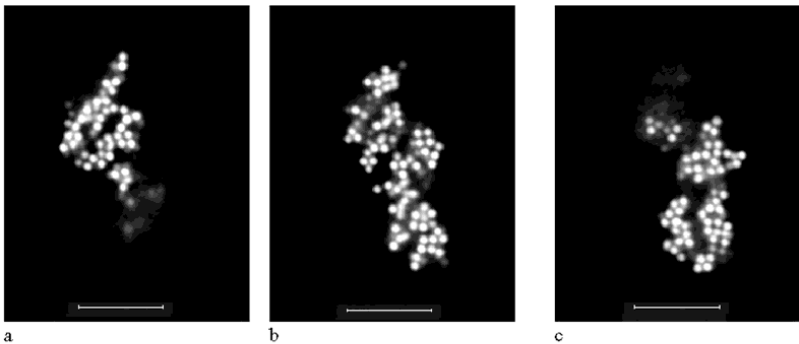


Microstructure subjected to compression and extension in shear flow.

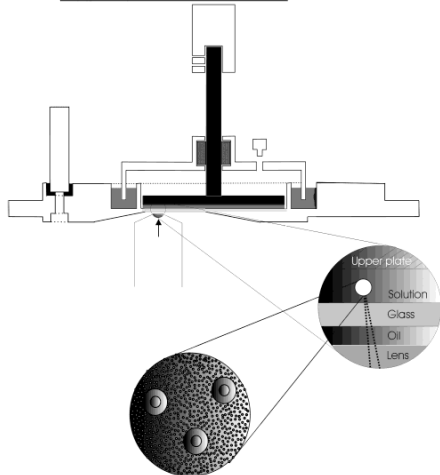
Effect of flow on structure

Flow affects the size, density and structural organization.

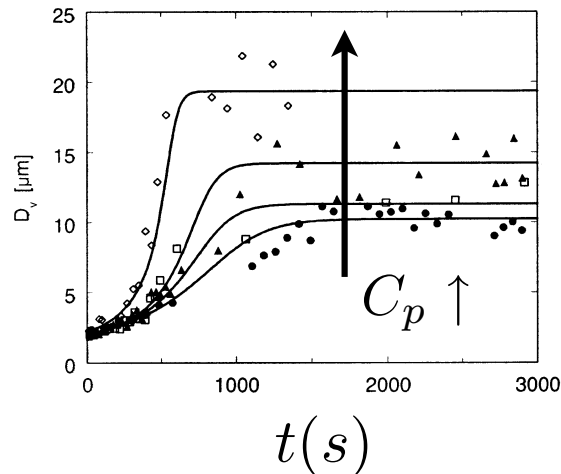
V. A. Tolpekin, M. H. G. Duits, D. van den Ende, and J. Mellema,
Langmuir 20, 2614 (2004).



$$\phi = 0.001 \quad d_f \approx 2.0$$



Average aggregate size

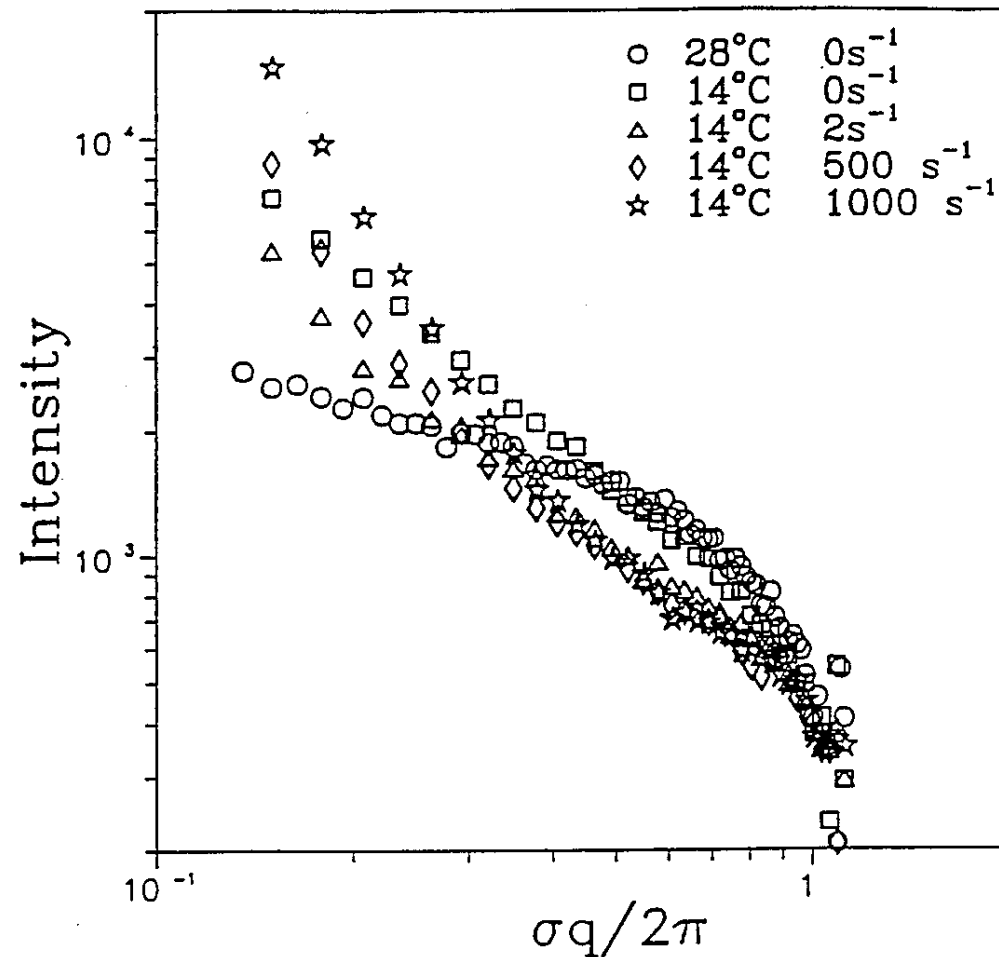


- Aggregate size determined by competition between attractive forces and hydrodynamic stresses.
- Aggregates larger with higher attraction, smaller with stronger shear.
- Fractal structure enables prediction of aggregation curve.

Compaction in flow

C. Rueb and C. Zukoski, J. Rheol. 41, 197 (1997).

Organophilic silica in tetradecane



Higher concentrations

“Butterfly” pattern

P. Varadan and M. Solomon,
Langmuir 17, 2918 (2001).

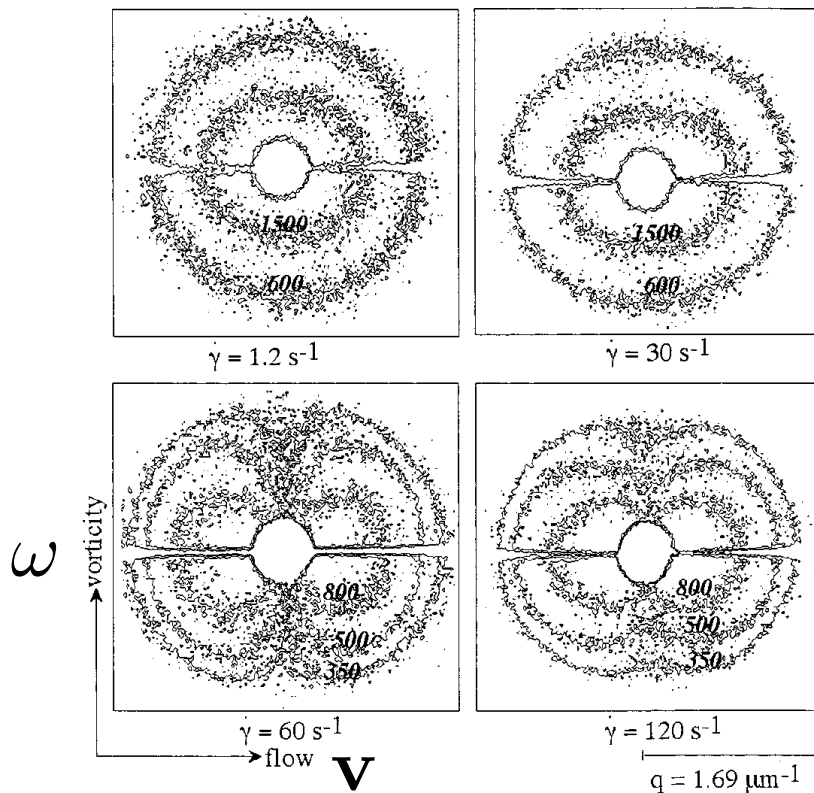
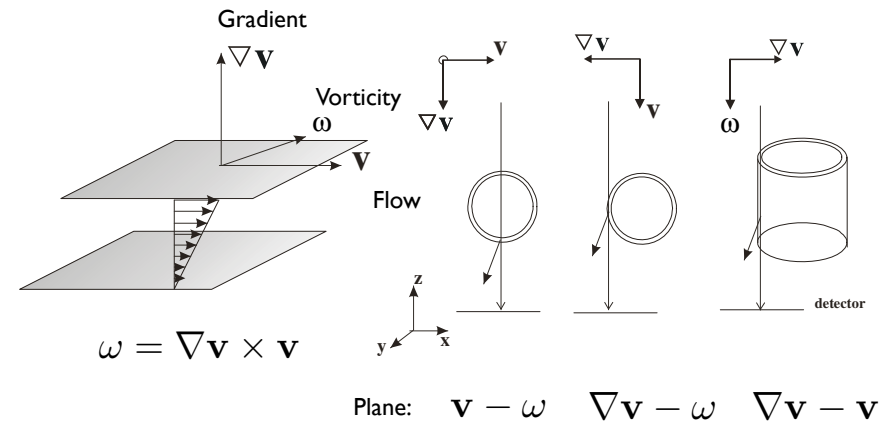
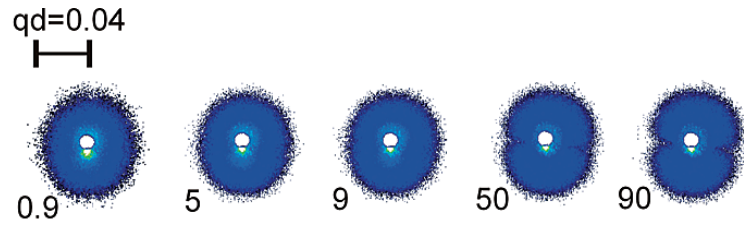


Figure 6. Isointensity contours showing the evolution of the anisotropy in the flow–vorticity plane at high shear rates for $\phi = 0.1$. The intensity values of the contours are shown in each image.

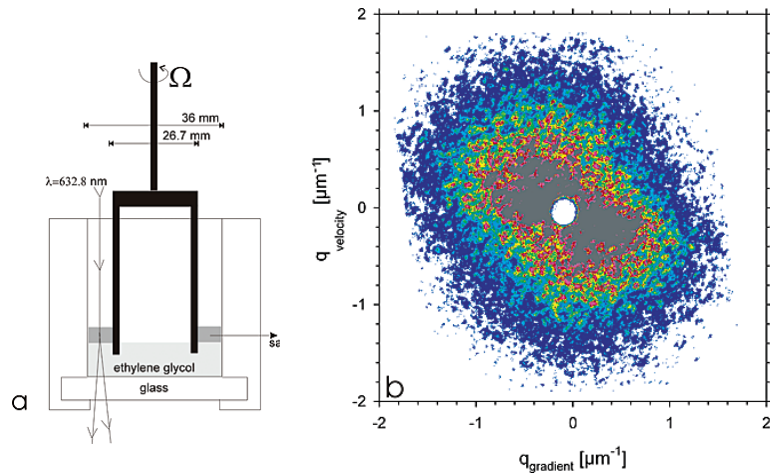


- Higher volume fractions, size reduction and flow densification are still observed.
- Self-similarity of the structure breaks down during shear flow.
- The microstructure becomes anisotropic.

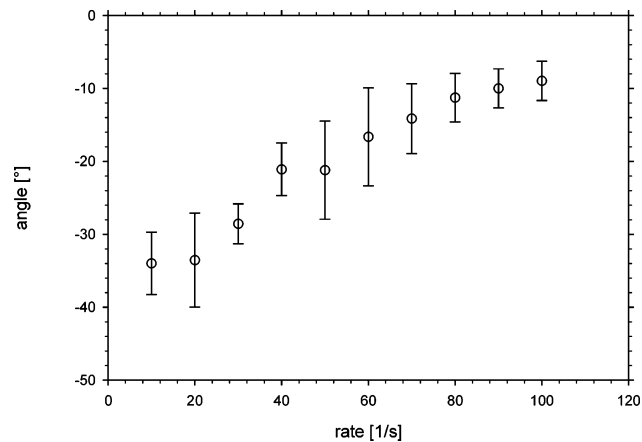
Scattering in gradient direction



Scattering in vorticity direction



Orientation in vorticity plane



Combined scattering results

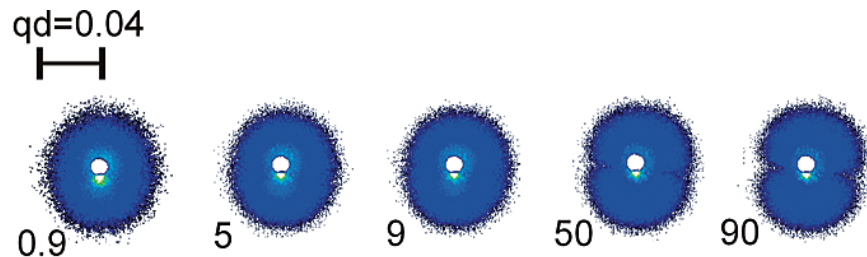
| | SAXS | USAXS | SALS |
|----------------------------|------|-----------------------------|------|
| ω v | | X | |
| ω $\dot{\gamma}$ | | X | X |
| $\dot{\gamma}$ v | X | $I_{\dot{\gamma}} \neq I_v$ | |

Figure 13. Overview of the structural information from the different scattering techniques during shear flow for a sticky sphere suspension. In the scattering planes marked with an X no information is available for the given scattering technique.

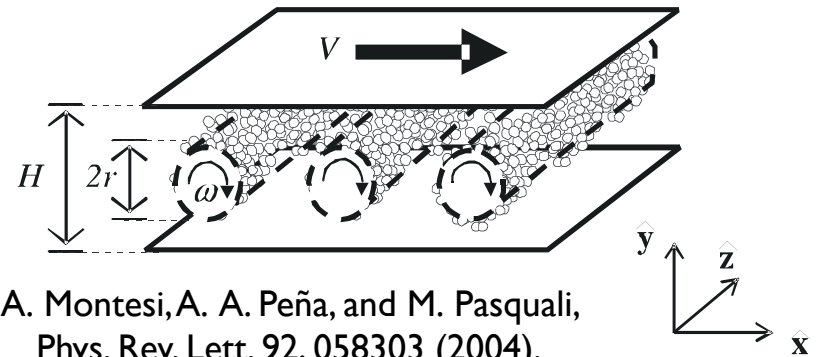
Structure is complex
and hierarchical

Proposed mechanisms

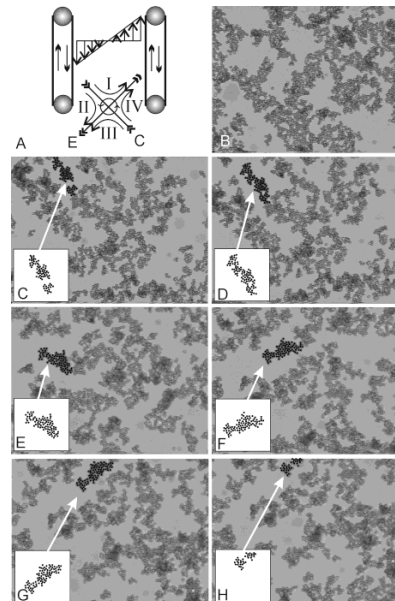
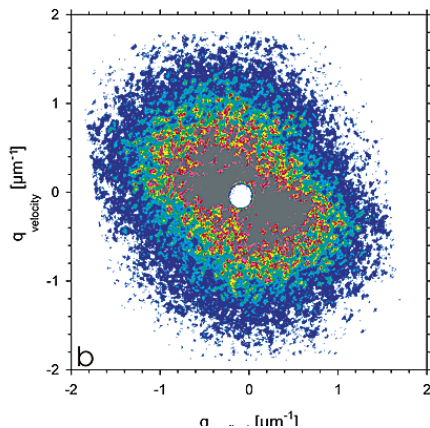
Velocity gradient direction



Rolling



Vorticity direction



Extension and compression

H. Hoekstra, et al. Langmuir,
19:9134–9141, 2003.

Structure in shear flow

H. Hoekstra, et al. Langmuir, 19:9134–9141, 2003.

- Apparent aggregate size during flow reveals weak dependence on shear rate and is direction dependent. A hierarchy of structures is present.
- Large scale structural inhomogeneity is induced by flow which leads to an anisotropic scattering patterns in the velocity gradient and vorticity planes. The magnitude of the anisotropy increases with increasing shear rate.
- The average orientation in the vorticity plane evolves from an orientation close to -45° toward the flow direction with increasing shear rate. The large length scale anisotropy and the anisotropic aggregate shape are explained by the directional dependence of aggregation and break-up processes.
- The direction dependent assembly and subsequent rupture also result in aggregates which are anisotropic in size, larger structures existing along the compression axis of the flow field, as shown by the USAXS measurements.
- The observed densification of the aggregates on a more local scale combined with the reversal of the local scale anisotropy observed in SAXS measurements, are consistent with the mechanism of structure formation. The aggregates are internally compressed when these larger scale structures are formed by compressing aggregates together.

Hierarchy and simple mechanism for many systems

Startup of steady shear

A. Mohraz and M. J. Solomon, J. Rheol. 49, 657 (2005).

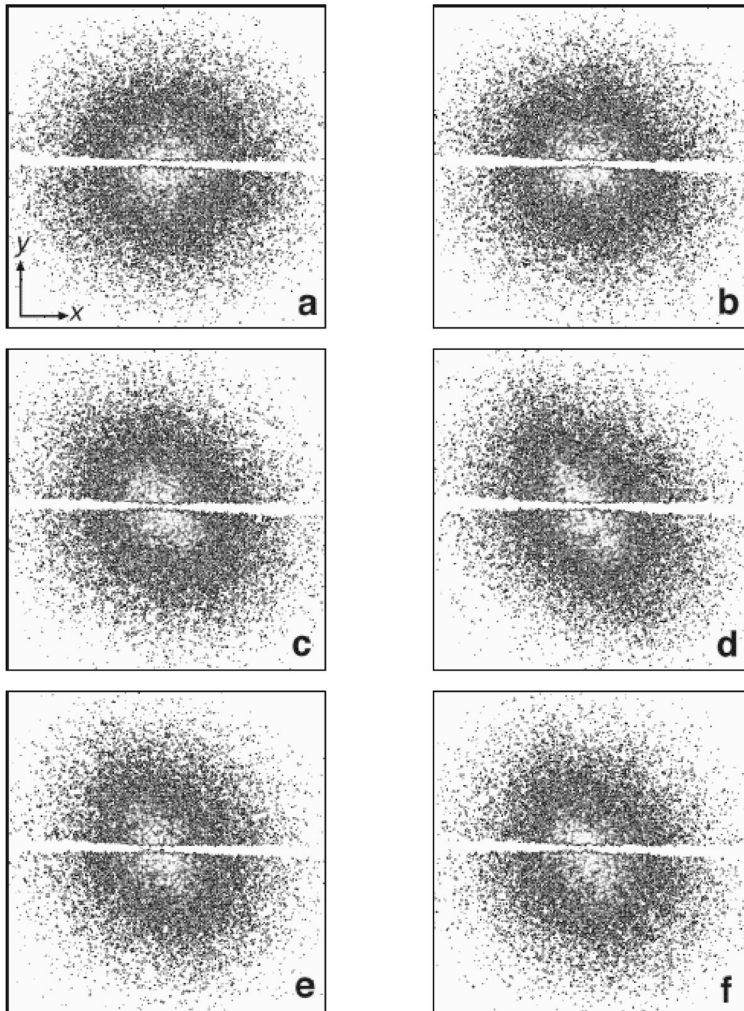
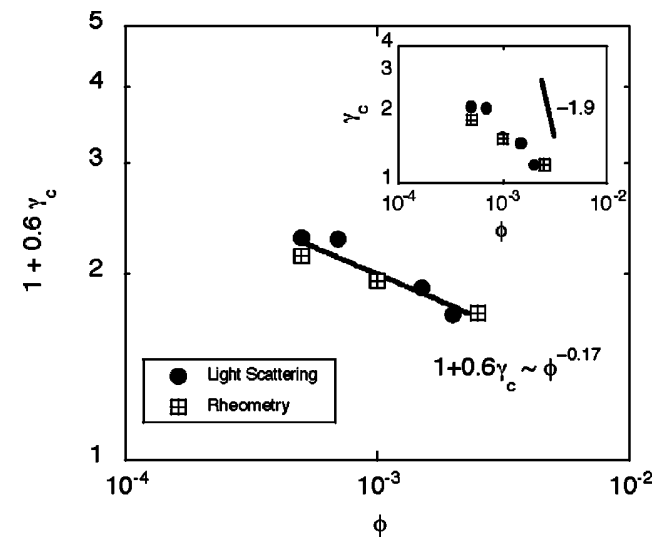


FIG. 4. Contour plots of a representative cascade of scattering patterns collected during start-up of steady shear flow of DLCA polystyrene gels with $\phi = 1.0 \times 10^{-3}$ and $\dot{\gamma} = 0.56 \text{ s}^{-1}$, and $t =$ (a) -0.1 , (b) 1.1 , (c) 2.2 , (d) 3.5 , (e) 6.3 , (f) 8.3 s. The time $t=0$ corresponds to the inception of shear. Maximum anisotropy is observed at ~ 3.5 s. The low-intensity region in the middle of images is due to the beam stop.

$$1 + 0.6\gamma_c \sim \phi^{(1-d_b)(3-d_f)}$$



- Scaling agrees with the simple model of a gel network that ruptures after the cluster backbone is extended affinely to its full length.
- Rheological measurements demonstrate that the maximum anisotropy coincides with a maximum in shear stress

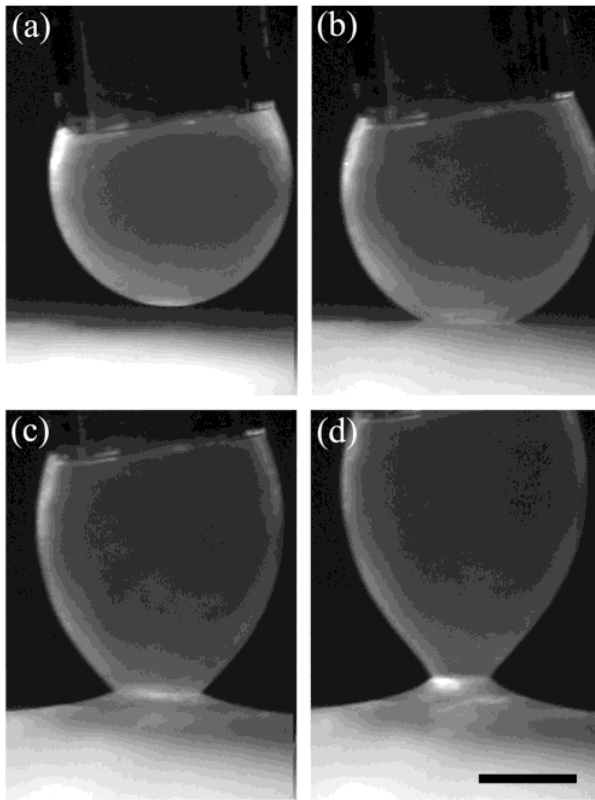
Gels at interfaces

Particles at interfaces

Stabilization of incompatible materials (blends, emulsions, foams)

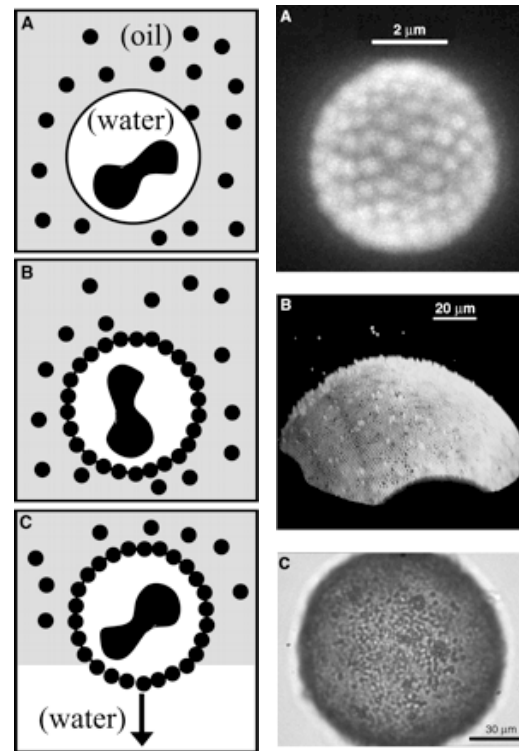
Pickering, J. Chem. Soc. 91, 2001, 1907

Interfacial mechanics



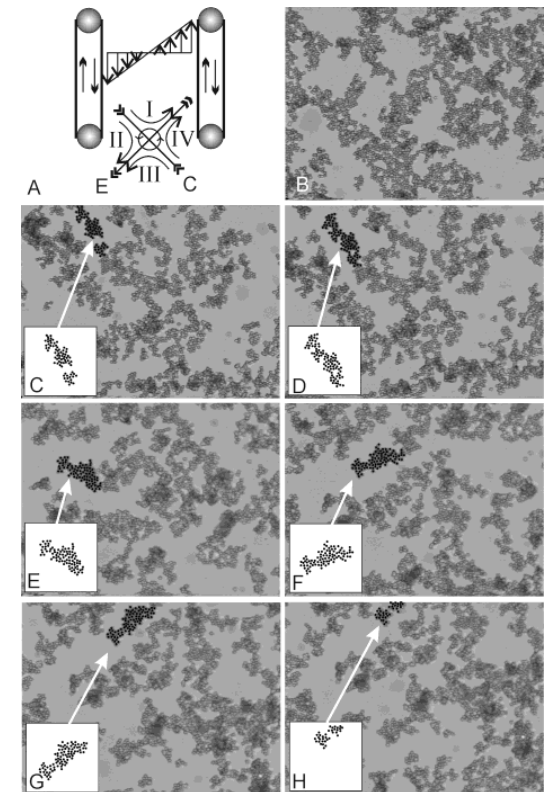
Stancick, et al. Langmuir, 20:90–94, 2004.

Structured materials



Dinsmore, A.D. Science, 298: 1006-1009 (2002).

Surface rheology

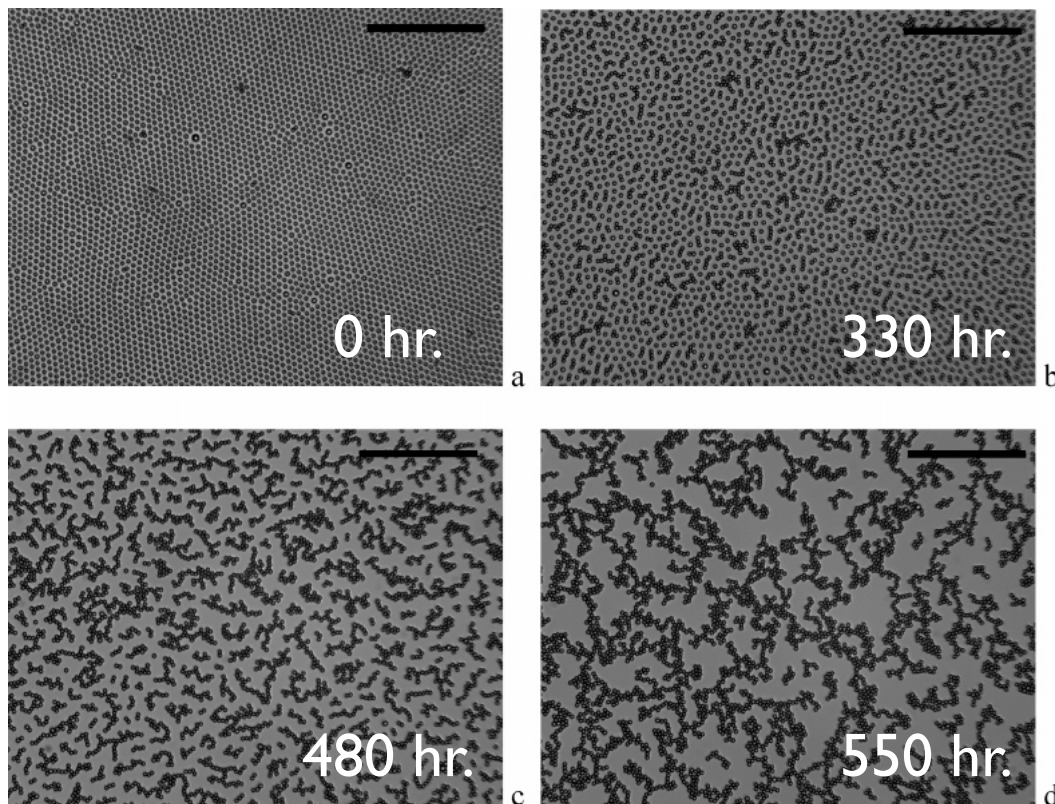


H. Hoekstra, et al. Langmuir, 19:9134–9141, 2003.

Aggregation phenomena

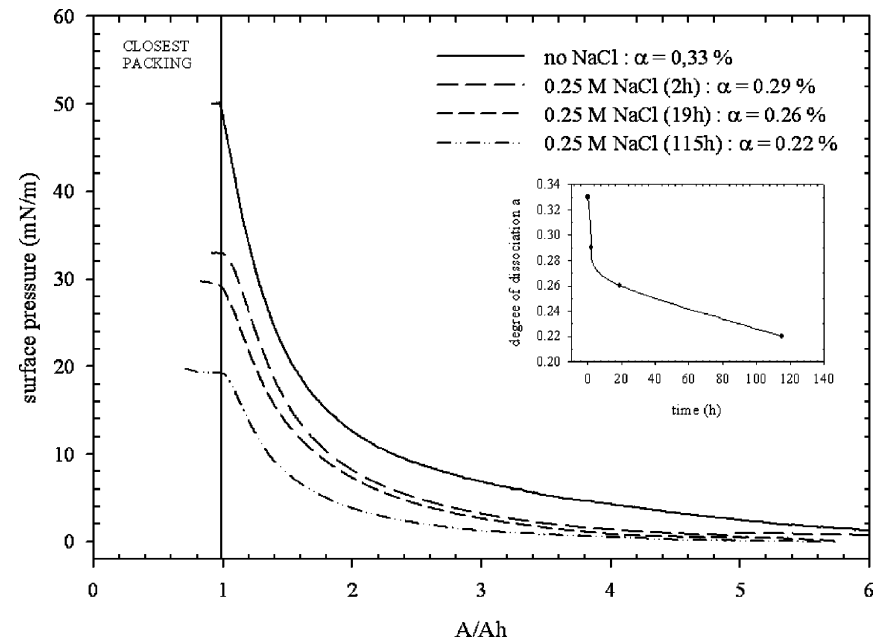
Decane-water (0.25M NaCl)

Reynaert and Vermant, Langmuir 22, 4936, 2006.



$$D_f = 1.58 \pm 0.03$$

Surface pressure isotherms



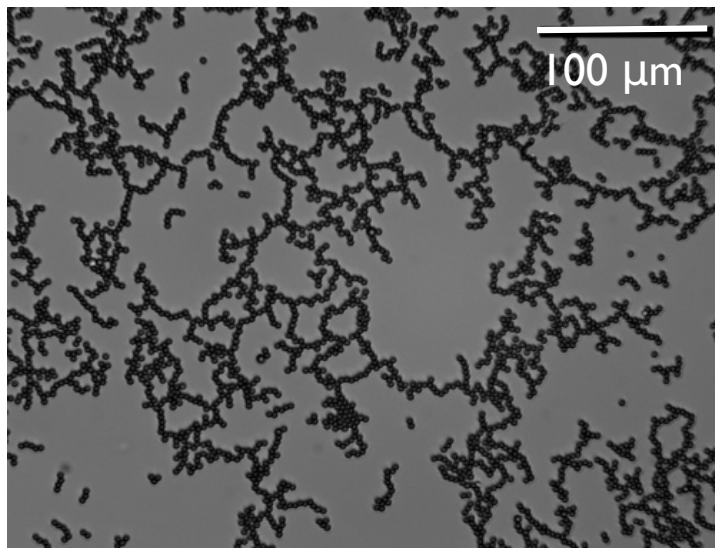
System becomes less repulsive with time

B. J. Park, et al. Langmuir 24, 1686 (2008).

Aggregation in presence of surfactants

Reynaert and Vermant, Langmuir 22, 4936, 2006.

Decane-(water + 0.5 mM SDS +
0.5 M NaCl) interface.

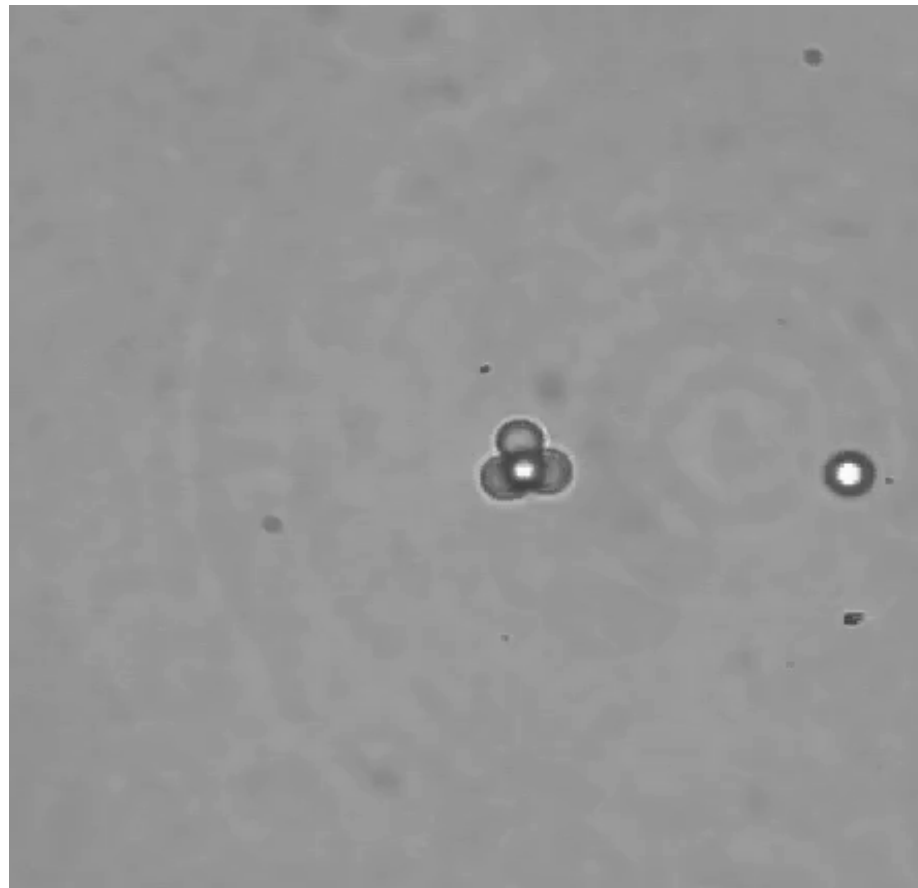
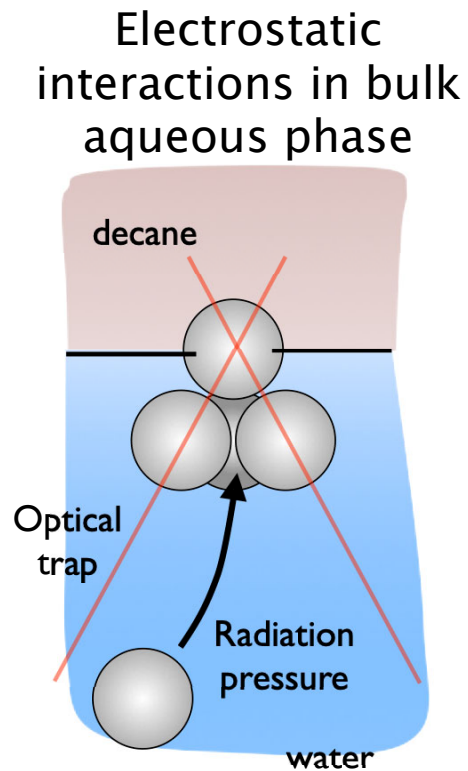


- Faster aggregation kinetics (hours instead of days)
- Lower fractal dimension (consistent with DLCA)

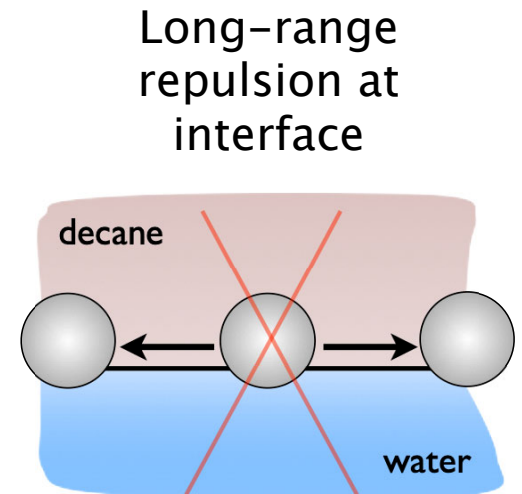
| $C_{\text{SDS}}[\text{mM}] +$ $C_{\text{NaCl}}[\text{M}]$ | ϕ | t_{IND} (min) | D_f | τ | ω | z |
|--|--------|---------------------------|-----------------|-----------------|---------------|---------------|
| 0.5 + 0 | 0.04 | >6000 | | | | |
| 0.5 + 0.1 | 0.1 | 330 | 1.44 ± 0.04 | 1.1 ± 0.1 | 2.8 ± 0.3 | 3.4 ± 0.4 |
| 0.5 + 0.3 | 0.05 | 275 | 1.45 ± 0.03 | 1.2 ± 0.1 | 2.1 ± 0.1 | 3.0 ± 0.1 |
| 0.5 + 0.5 | 0.11 | 40 | 1.46 ± 0.03 | 1.7 ± 0.1 | 0.5 ± 0.1 | 1.3 ± 0.1 |
| 0.1 + 0.25 | 0.08 | 1000 | 1.47 ± 0.03 | 1.49 ± 0.05 | 3.7 ± 0.4 | 4.9 ± 0.5 |
| 0.9 + 0.3 | 0.08 | 290 | 1.46 ± 0.04 | 0.9 ± 0.1 | 2.7 ± 0.2 | 2.8 ± 0.5 |

Electrostatic interactions

Polystyrene particles at decane-water interface
 $2a = 3.1 \pm 0.1 \mu\text{m}$, $\sigma = 7.4$ or $9.1 \mu\text{C}/\text{cm}^2$

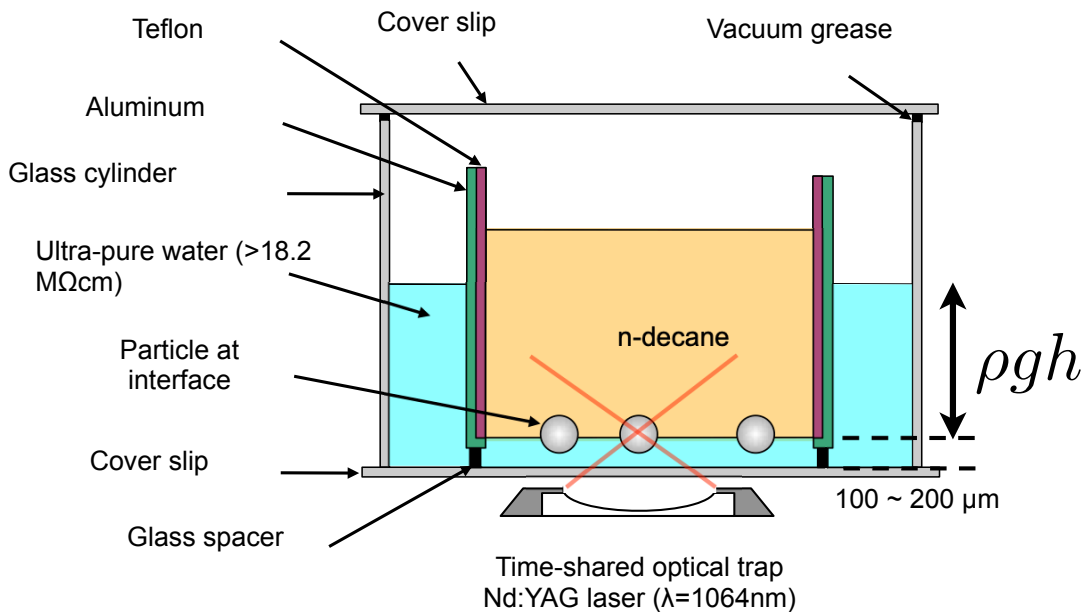


$15\mu\text{m}$

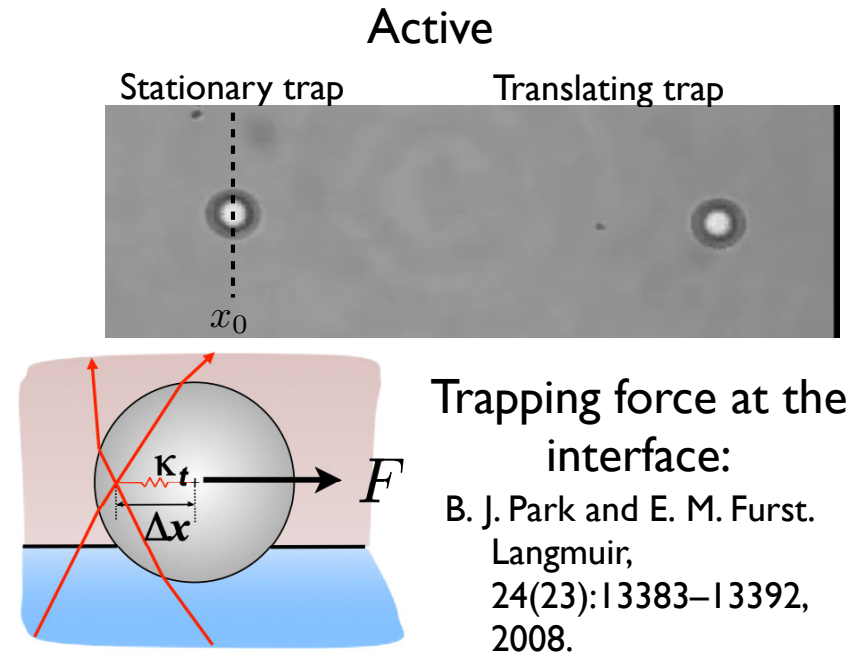


Particle pair interaction measurements using laser tweezers

Experimental setup



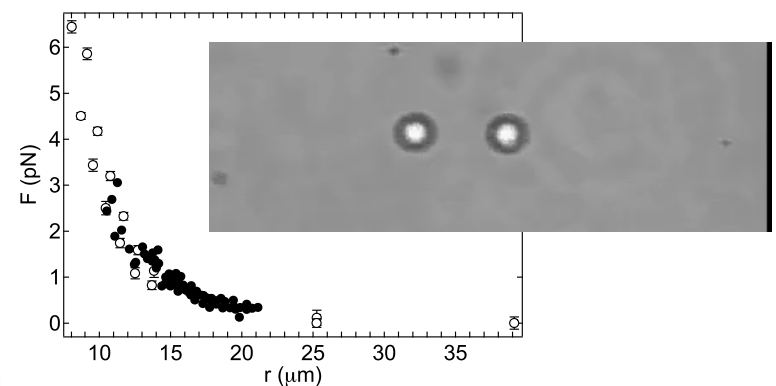
Interaction measurements



For reproducibility:

1. n-decane: rinsed over aluminum oxide support
2. Particles: repeated centrifugation and re-dispersion
3. Cover slip flame treated: contact angle ~ 0 degrees

Passive: Force from trajectories

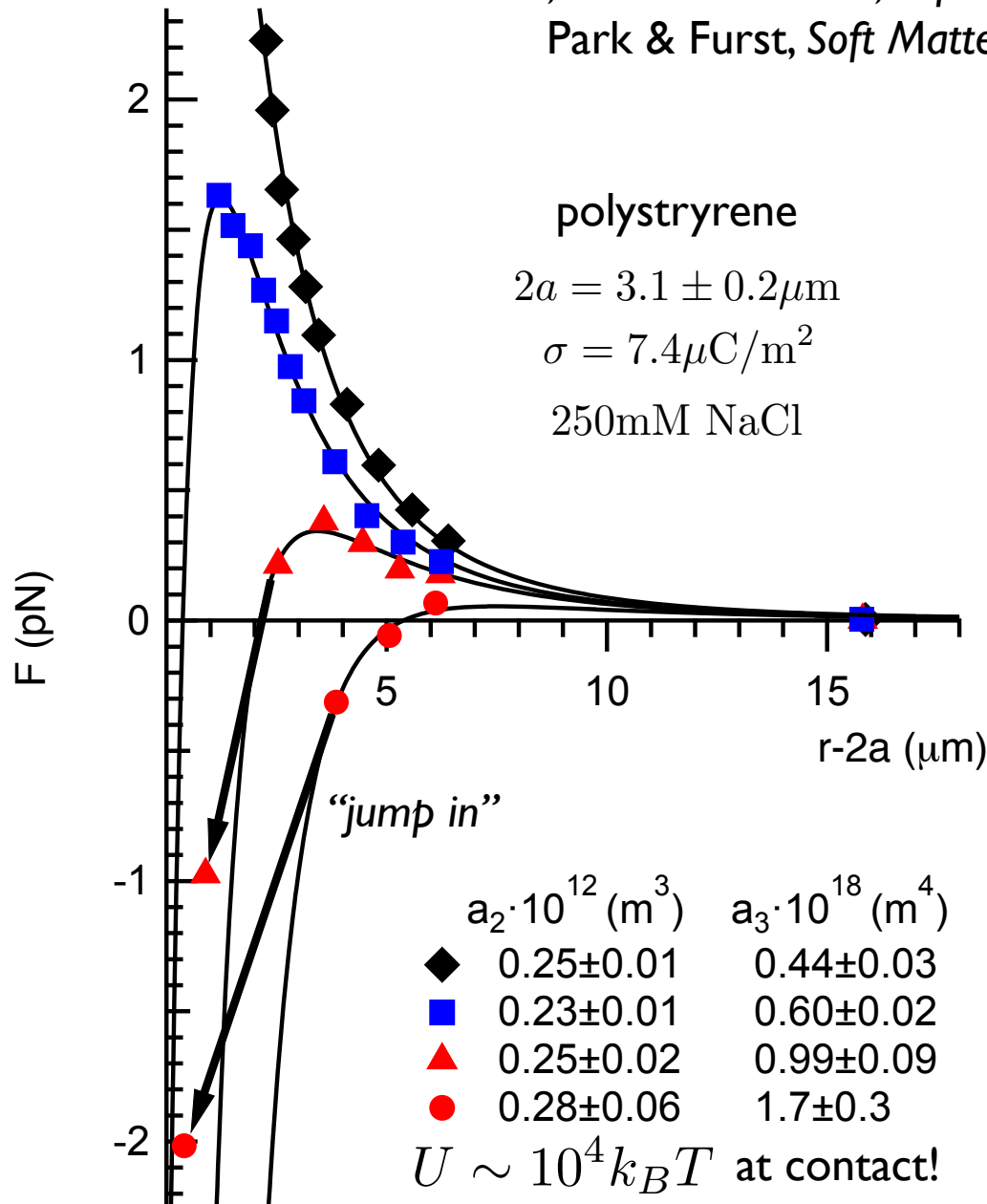


Interaction potential & force

Park, B. J. et al. *Langmuir* 24, 1686–1694 (2008).

Park, Vermant & Furst, *Soft Matter* 6, 5327–5333 (2010).

Park & Furst, *Soft Matter* 7, 7676–7682 (2011).



$$\frac{U(r)}{k_B T} = \frac{a_2}{r^3} - \frac{a_3}{r^4}$$

$$F(r) = \frac{3a_2 k_B T}{r^4} - \frac{4a_3 k_B T}{r^5}$$

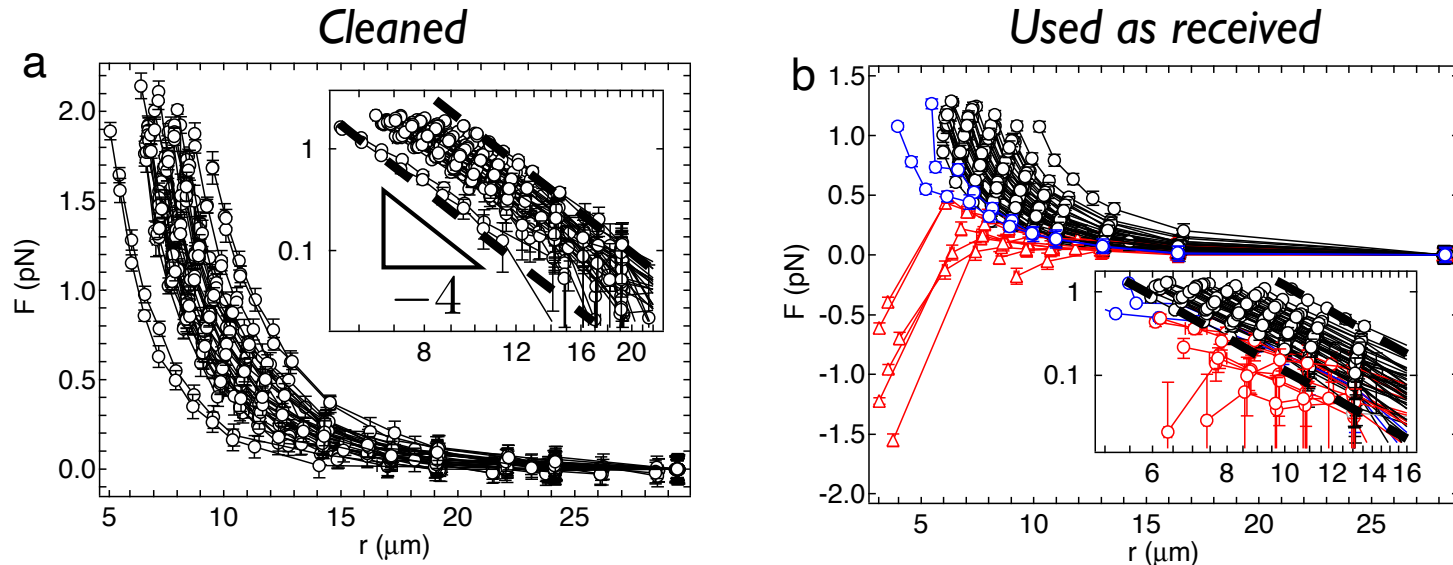
“Heterogeneous” – depends on particle pair
 Sensitive to salts, surfactants, and particle prep

Variation of interaction

Park, Vermant & Furst, *Soft Matter* 6, 5327–5333 (2010).

Park & Furst, *Soft Matter* 7, 7676–7682 (2011).

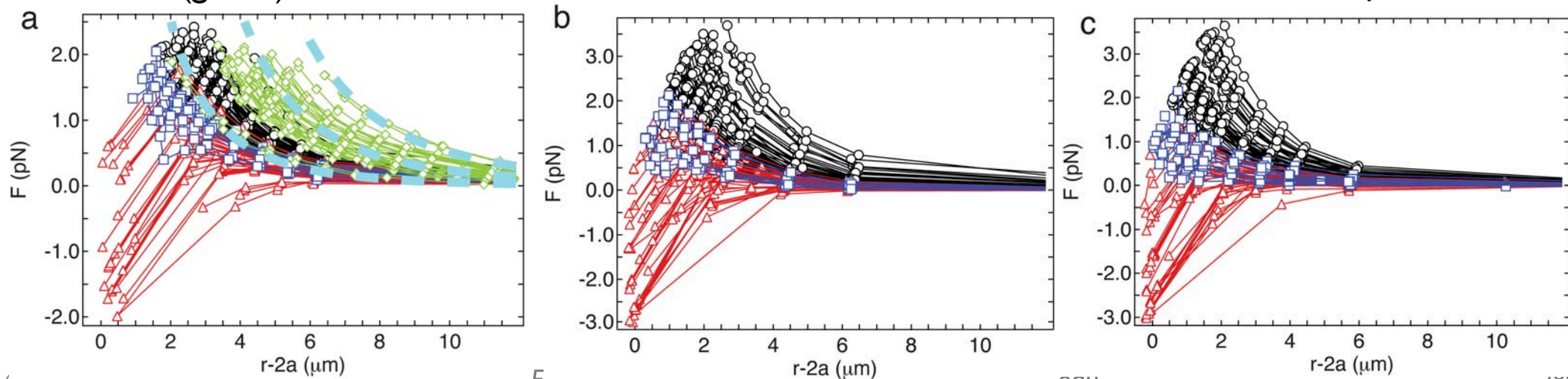
Neat (no salt or surfactant)



Neat (green) or 0.25 M salt

0.25 M salt + 0.1 mM SDS

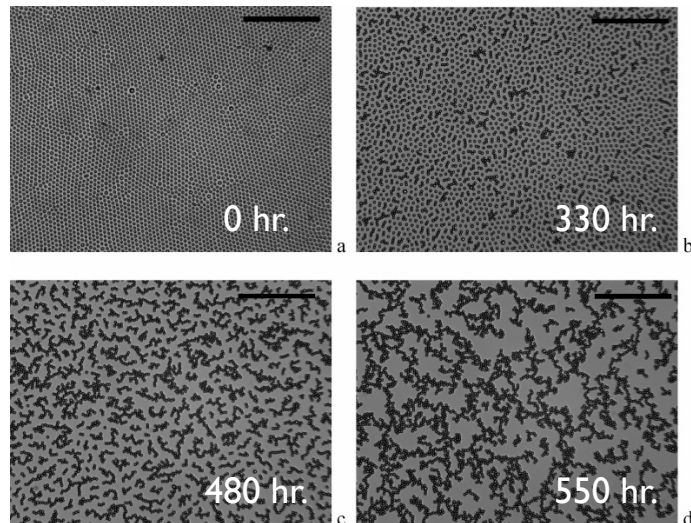
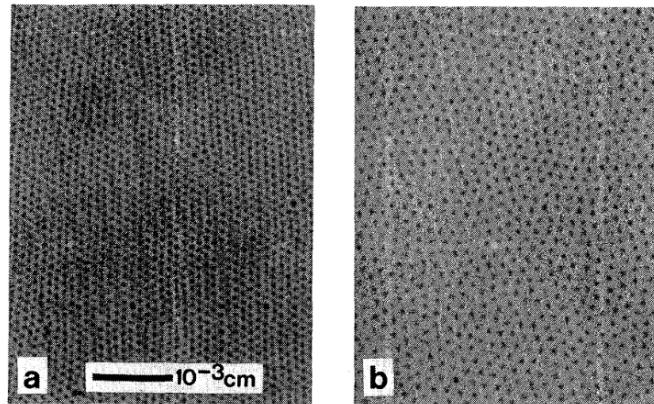
0.25 M salt + 25 μM SPAN 80



Electrostatics at the interface: Dipole repulsion

2D crystal

Pieranski, Phys. Rev. Lett. 45, 569, 1980.

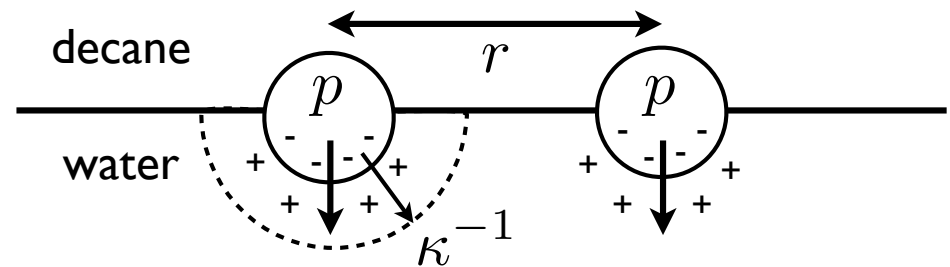


Reynaert and Vermant, Langmuir 22, 4936, 2006.

Stable for weeks—large kinetic stability barrier

Charge dissociation model

Hurd, J. Phys. A, 18, 1055, 1985.



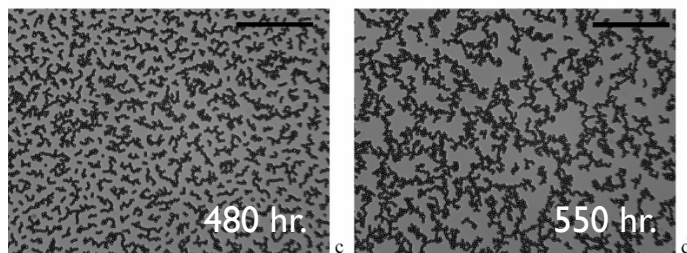
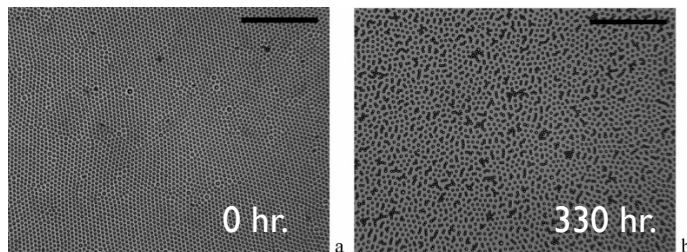
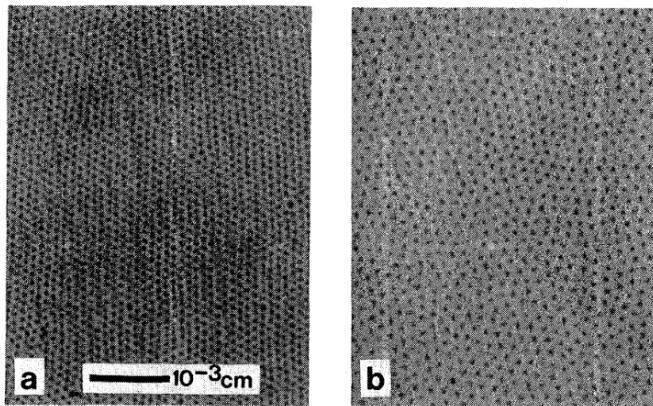
$$U(r) = \frac{\epsilon_{oil} q_{water}^2}{2\pi\epsilon_0\epsilon_{water}^2\kappa^2 r^3}$$

Charge renormalization

Weaker salt dependence than Hurd model

2D crystal

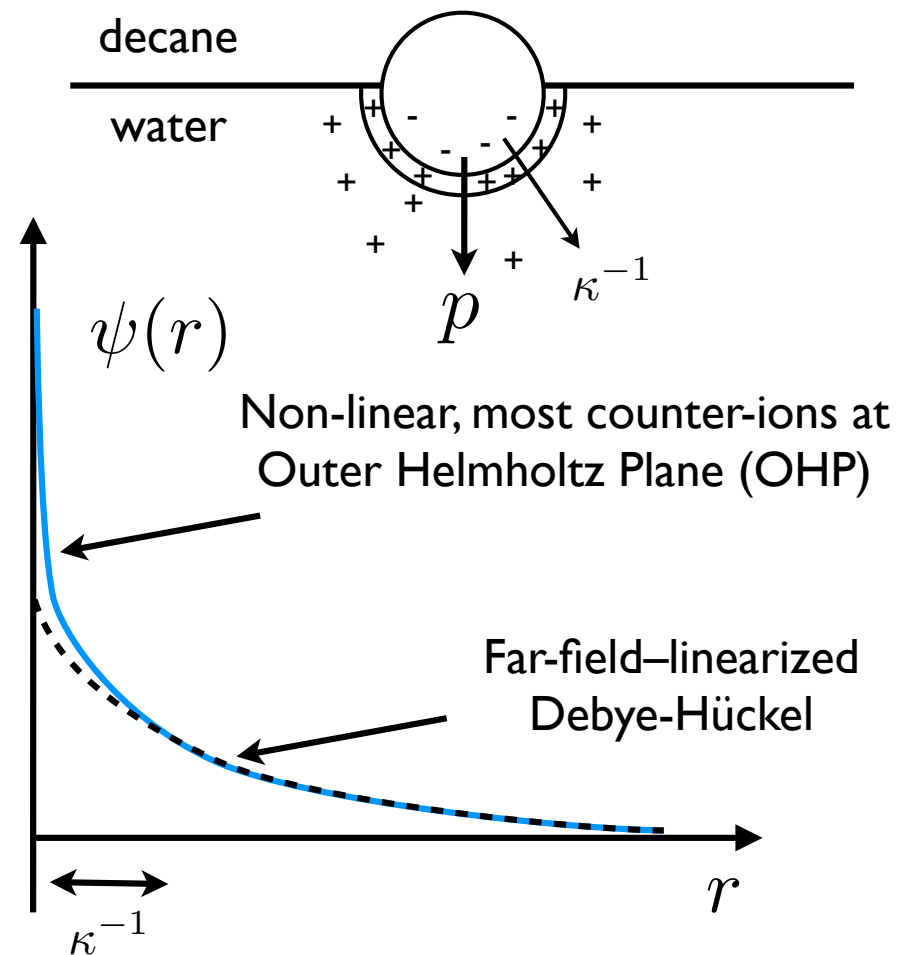
Pieranski, *Phys. Rev. Lett.* 45, 569, 1980.



Reynaert and Vermant, *Langmuir* 22, 4936, 2006.

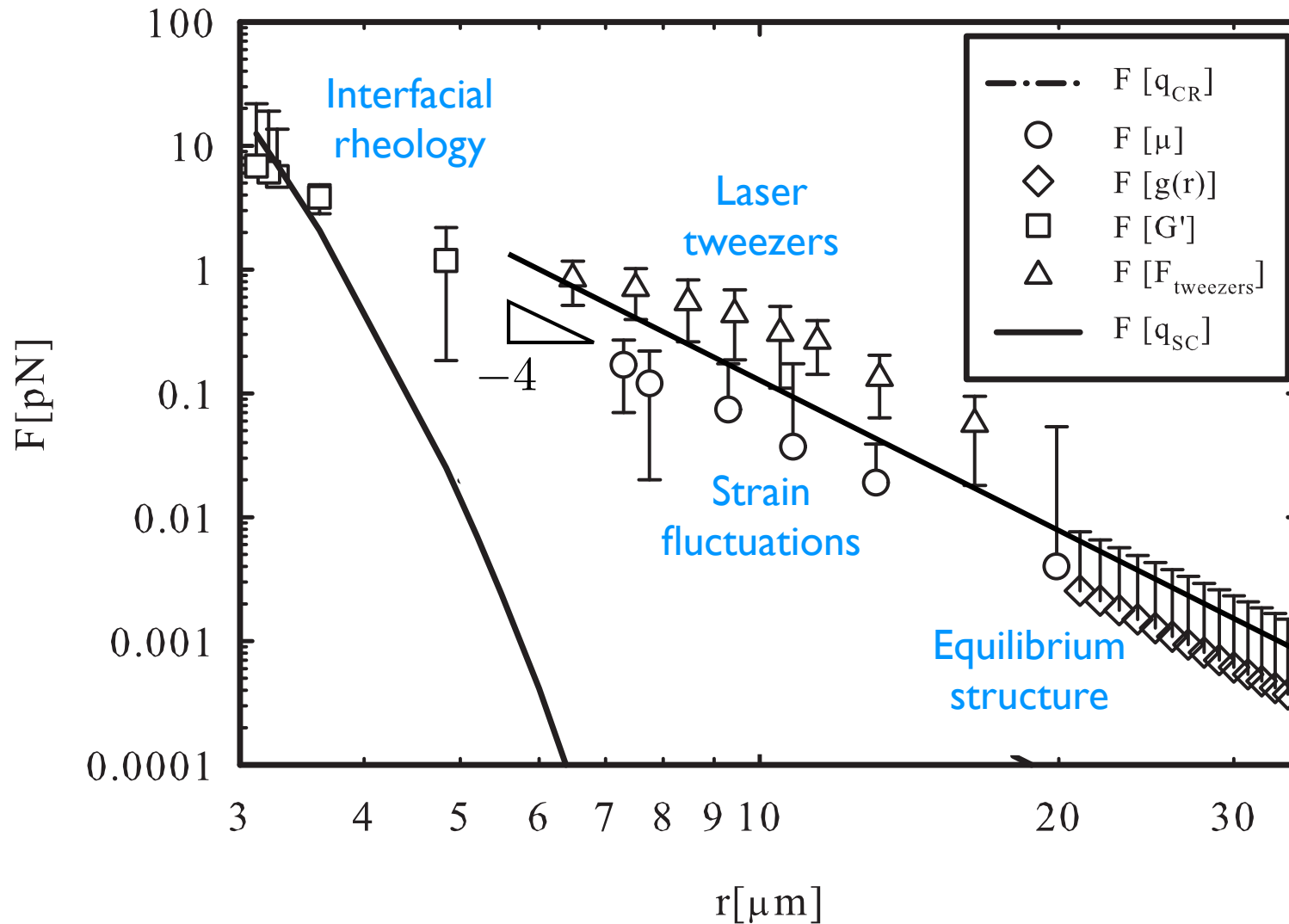
D. Frydel et al. *Phys. Rev. Lett.* 99, 118302, 2007.

$$q_{\text{eff}} = g(\kappa R)q$$



Consensus experiments

Masschaele, Park, Fransaer, Furst and Vermant, *Phys. Rev. Lett.*, 105:048303, 2010.

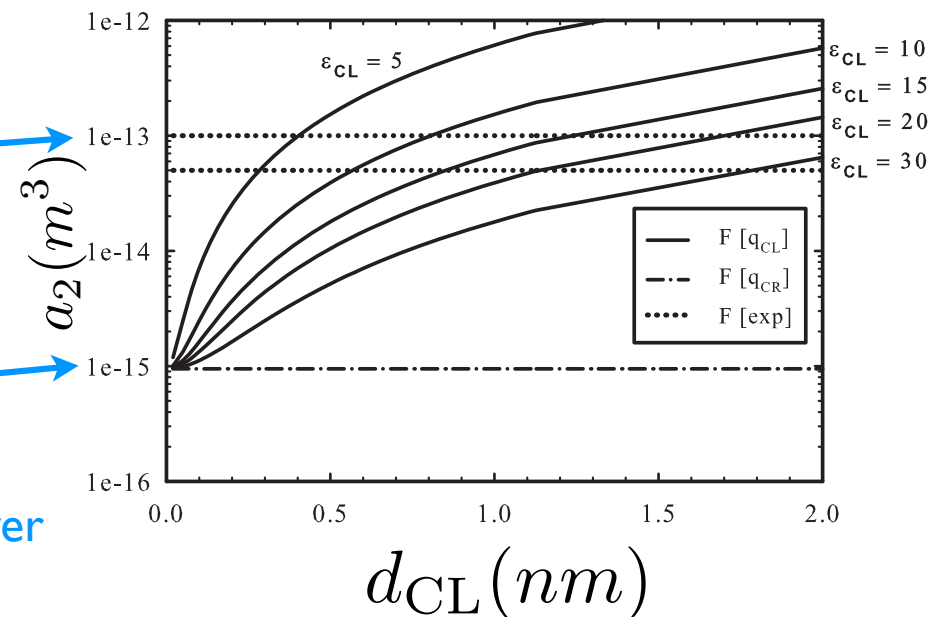
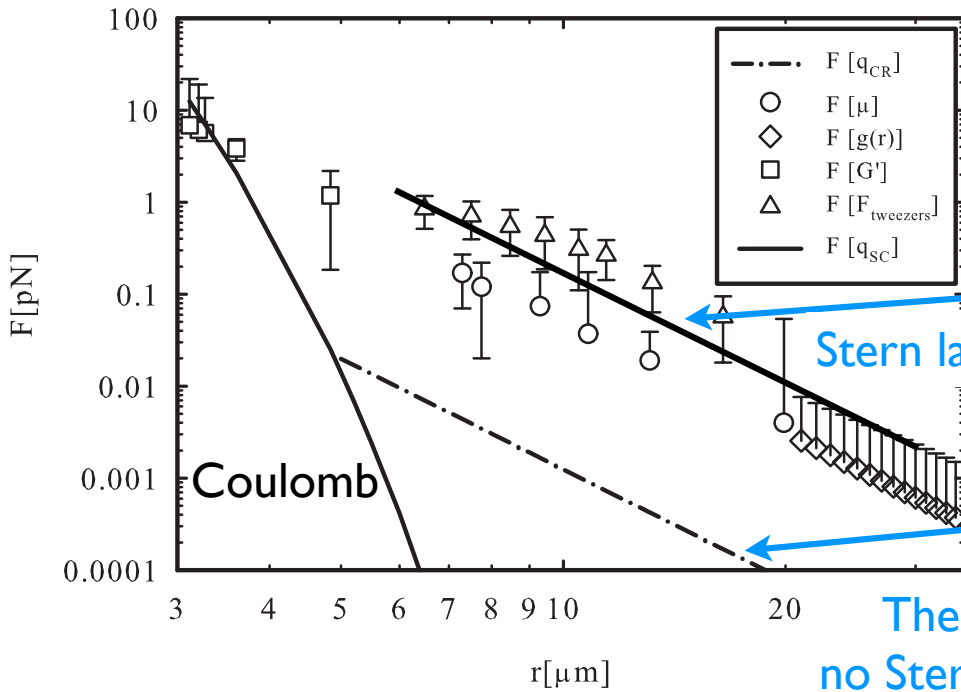
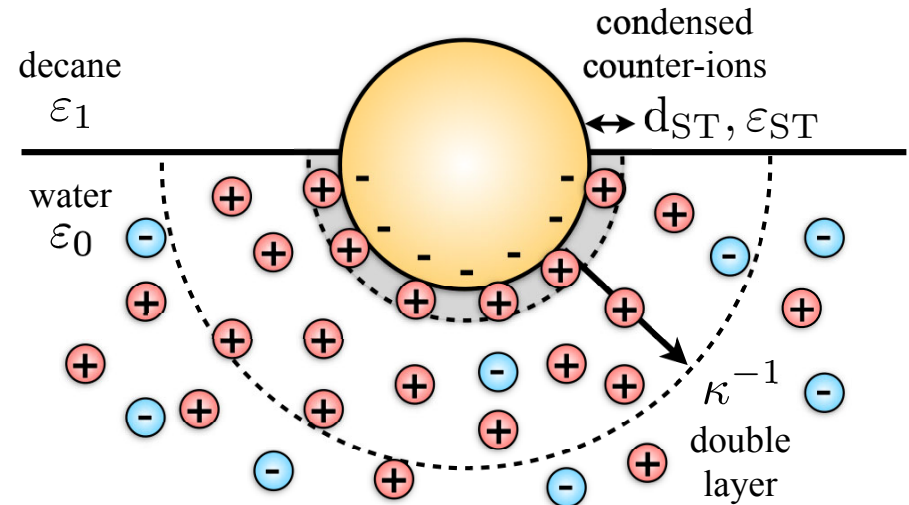


Contribution of Stern layer

Masschaele, Park, Fransaer, Furst and Vermant, *Phys. Rev. Lett.*, 105:048303, 2010.

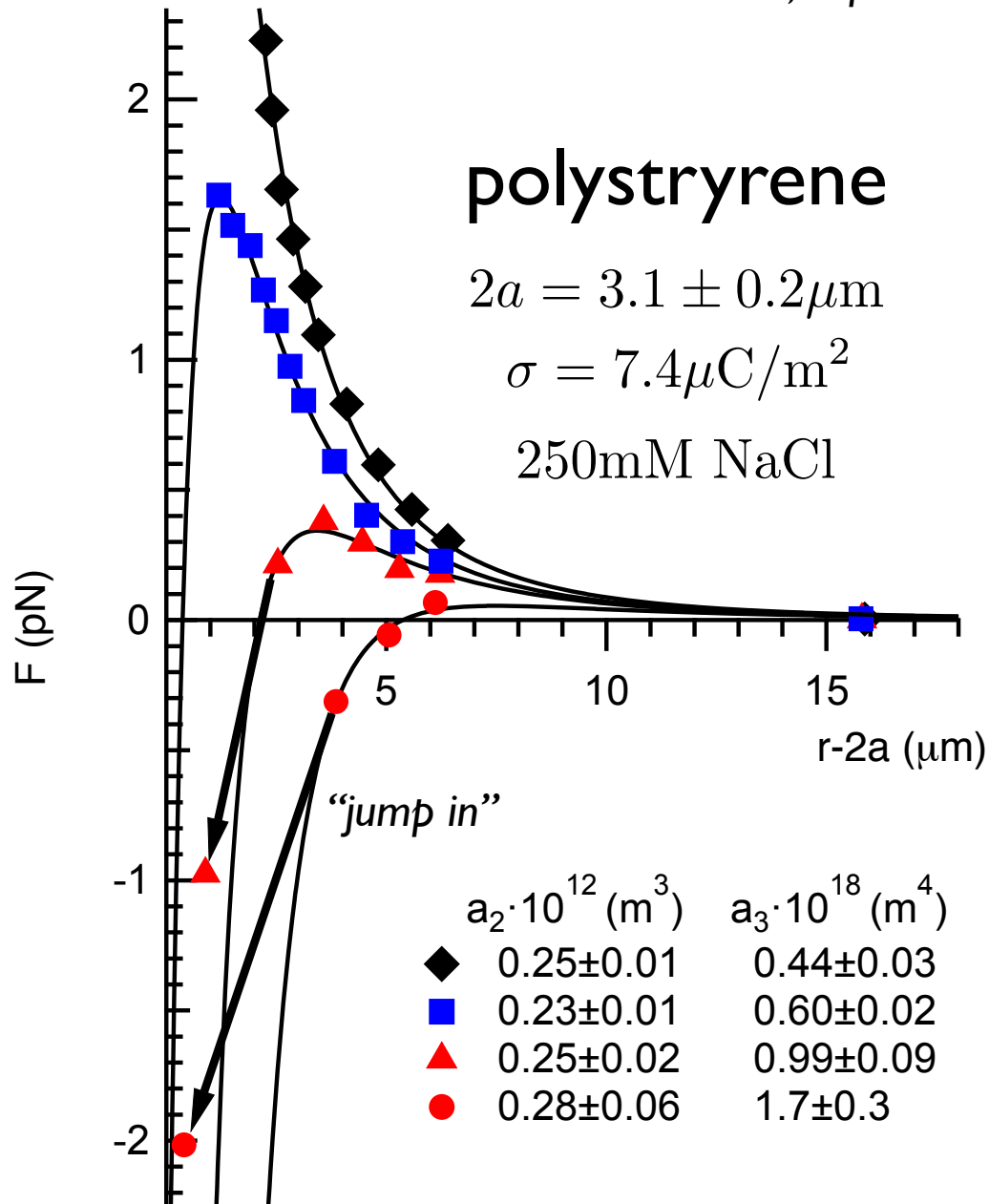
$$F = \frac{3a_2 k_B T}{r^4}$$

Four independent measurements:
Tweezers, equilibrium structure,
surface rheology, dynamics



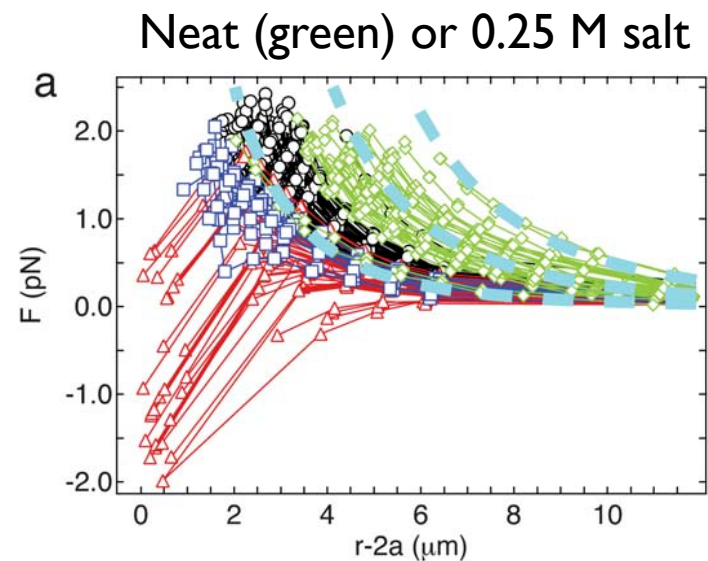
Attractive interaction

Park & Furst, *Soft Matter* 7, 7676–7682 (2011).



$$\frac{U(r)}{k_B T} = \frac{a_2}{r^3} - \frac{a_3}{r^4}$$

$$F(r) = \frac{3a_2 k_B T}{r^4} - \frac{4a_3 k_B T}{r^5}$$



Interaction parameter distributions

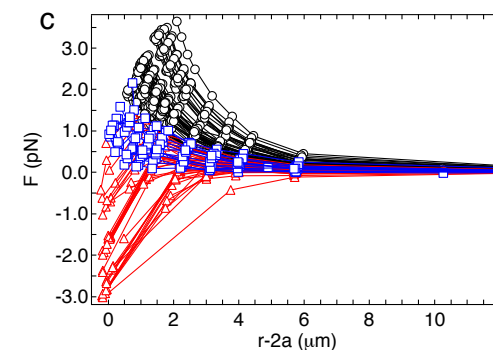
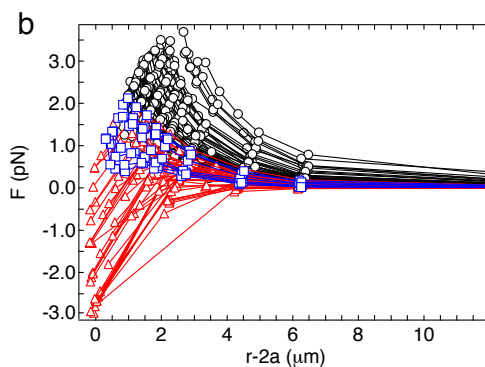
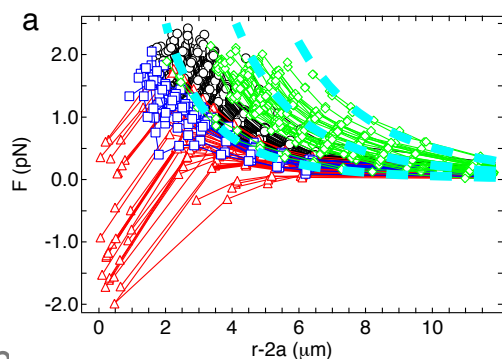
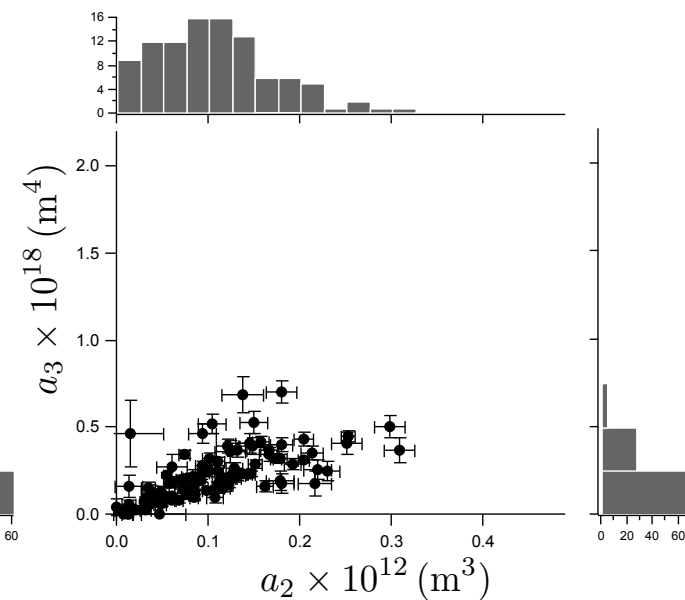
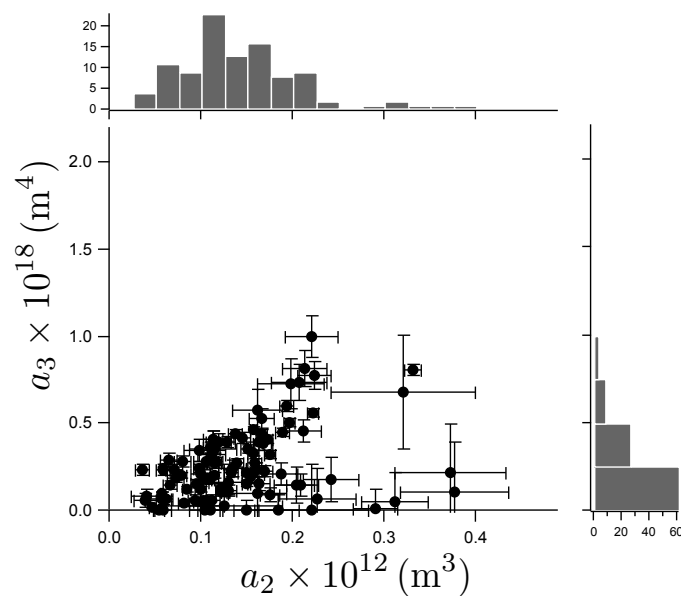
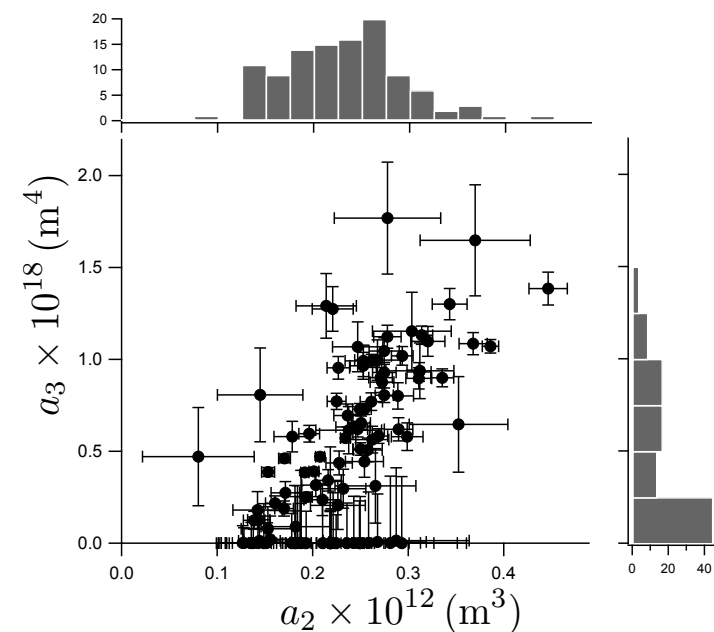
Park & Furst, *Soft Matter* 7, 7676–7682 (2011).

$$F_{\text{cap}} = -\frac{4a_3k_B T}{r^5} \quad F_{\text{rep}}(r) = \frac{3a_2k_B T}{r^4}$$

NaCl

SDS / NaCl

SPAN 80

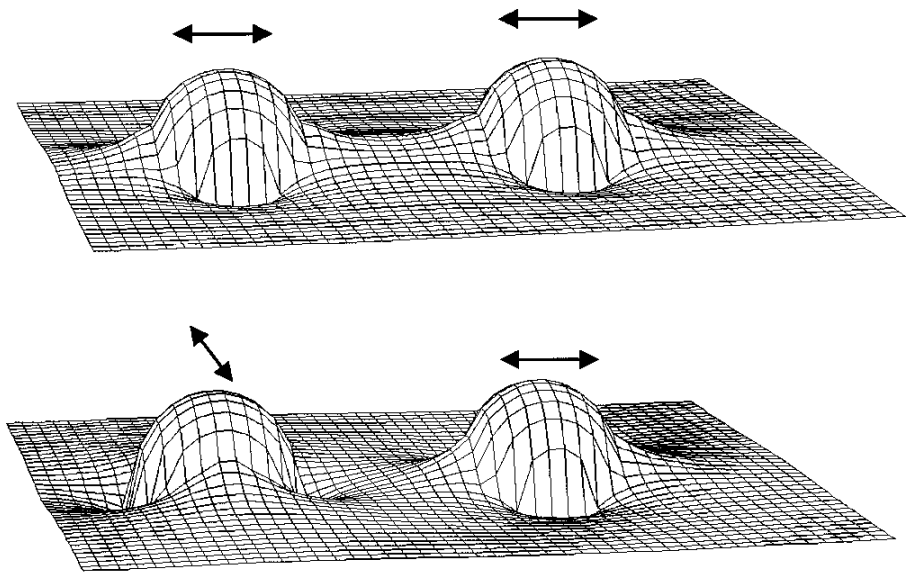


Capillary forces

D. Stamou, et al. Phys. Rev. E, 62:5263–5272, 2000.

Far-field: quadrupolar interaction

Contact line roughness



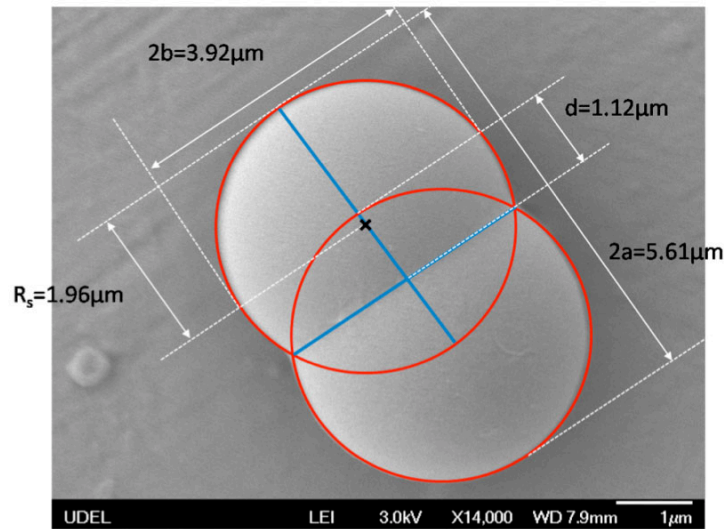
$$U_c = -12\pi\gamma H_2^2 \cos[2(\phi_A + \phi_B)] \left(\frac{r_c}{r}\right)^4$$

$$F(r) = -\frac{4a_3 k_B T}{r^5} \quad a_3 = 12\pi\gamma a^4 H_2^2 \quad H_2 \approx 45\text{nm}$$

Forced irregular contact line

Park & Furst, *Soft Matter* 7, 7676–7682 (2011).

PS doublets



H. R. Sheu, et al. *J. Poly. Sci. A*,
28:629–651, 1990.

Thanks: E. Dufresne and Jin-Gyu Park,
Yale University

$$F(r) = -\frac{4a_3 k_B T}{r^5}$$

Capillary attraction

Trap and release with optical tweezers

